Angle-dependent identification of PMSM HF-parameters with large bandwidth based on switching harmonics of a 2-level inverter

Johannes Stoß
Elektrotechnisches Institut (ETI)
Karlsruhe Institute of Technology (KIT)
Karlsruhe, Germany
johannes.stoss@kit.edu

Benedikt Schmitz-Rode
Elektrotechnisches Institut (ETI)
Karlsruhe Institute of Technology (KIT)
Karlsruhe, Germany
benedikt.schmitz-rode@kit.edu

Philipp Steimel
Elektrotechnisches Institut (ETI)
Karlsruhe Institute of Technology (KIT)
Karlsruhe, Germany
steimel.philipp@web.de

Hassen Aouadi
Elektrotechnisches Institut (ETI)
Karlsruhe Institute of Technology (KIT)
Karlsruhe, Germany
hassen.aouadi@kit.edu

Dr.-Ing. Andreas Liske
Elektrotechnisches Institut (ETI)
Karlsruhe Institute of Technology (KIT)
Karlsruhe, Germany
andreas.liske@kit.edu

Prof. Dr.-Ing. Marc Hiller
Elektrotechnisches Institut (ETI)
Karlsruhe Institute of Technology (KIT)
Karlsruhe, Germany
marc.hiller@kit.edu

***Abstract* — This paper presents a new method for identifying angle-dependent high frequency (HF) machine parameters using the current- and voltage harmonics of a 2-level voltage source inverter. By utilizing existing excitations, an additional test signal can be omitted. This reduces the implementation effort and increases the maximum evaluation frequency beyond 100 kHz.**

Keywords — modelling, measurement, test bench, brushless drive

I. Introduction

Permanent magnet synchronous machines are suitable for a wide range of applications due to their high power density and efficiency. To operate these machines cost-effectively with high electromagnetic and thermal utilization, the condition and state of the machine must be monitored at all times.

For this purpose, various methods have been developed using HF machine characteristics [1]. The high-frequency properties of the machine are significantly influenced by iron and copper losses. While the frequency-dependent iron and winding losses lead to higher resistances [2], the eddy currents lead to lower inductances [3]. During characterization, the frequency dependence of the inductances and resistances are examined with regard to the parameters to be estimated, like rotor angle, temperature or torque.

In order to operate machines closer to the thermal limit without demagnetizing the rotor, temperature monitoring is required. Since a direct temperature measurement in the rotor is very complex, an estimation of the magnet temperature using its HF properties can lead to a reduction of the overall system complexity and costs [4, 5].

As the HF characteristics have a strong angular dependence, the HF-resistance [6] as well as the HF-inductance [1, 7] can be used to determine the rotor angle. By measuring and modelling these HF effects, the overall angle detection accuracy can be increased [2]. In addition, torque estimation using the HF inductance is also possible [8].

Most of these estimation methods require exact parameterization of the HF models in advance to determine the state of the system based on the respective measurement signal. Typically, the parameters are determined by measurement with an additional test signal or FEM simulation. The measurements depend on the test signal frequency and would therefore have to be carried out successively for different frequencies to allow identification for a large bandwidth. This significantly increases the effort required to measure a large frequency range and limits the maximum frequency to 2 kHz [1].

This paper therefore proposes a new approach. To avoid an additional signal injection for identifying high frequency machine parameters, the existing current- and voltage harmonics of a voltage source inverter are evaluated. This allows the bandwidth of the measurement to be significantly extended.

Due to the high bandwidth of the switching harmonics, the identification can be carried out at several frequencies at the same time, providing a simple and yet powerful method for angle-dependent parameter identification with high bandwidth. In the next section the HF machine model and the new identification scheme are presented.

II. High frequency machine Model

The HF machine characteristics with locked rotor can be described as follows:

$$\begin{bmatrix} u_\mathrm{d} \\ u_\mathrm{q} \end{bmatrix} = \begin{bmatrix} R_\mathrm{HF,dd} & R_\mathrm{HF,dq} \\ R_\mathrm{HF,qd} & R_\mathrm{HF,qq} \end{bmatrix} \begin{bmatrix} i_\mathrm{d} \\ i_\mathrm{q} \end{bmatrix} + \begin{bmatrix} L_\mathrm{dd} & L_\mathrm{dq} \\ L_\mathrm{qd} & L_\mathrm{qq} \end{bmatrix} \frac{d}{dt} \begin{bmatrix} i_\mathrm{d} \\ i_\mathrm{q} \end{bmatrix} \qquad (1)$$

In contrary to HF models shown in [2], the HF- and DC-resistors are not considered separately, but as one resistor. This approach is chosen because an additional DC test signal will not be applied in the further measurement procedure, which means that a simple distinction between DC and HF resistors is neither possible nor necessary. Furthermore, it is assumed that $L_\mathrm{dq} = L_\mathrm{qd}$. This reduces the number of parameters to be identified to 7. In contrast to the rotating fundamental wave model, the shown locked rotor HF model does not consider induced voltages due to the permanent magnet flux. Based on this model, the following section will now describe the identification procedure for locked rotor measurement of angle, frequency and current dependent machine parameters.

III. Identification Principle

To be able to determine the frequency-dependent machine parameters, the identification is carried out at standstill for all rotor angles to be measured. For this, it is first necessary to determine the initial rotor position angle in order to carry out the park transformation and identifying the dq machine parameter.

A. Determination of the initial orientation

Like the methods presented in [9] the angle estimation is performed using a sinusoidal voltage excitation in stationary reference frame. The methods presented are mostly based on a simplified machine modelling which was published in [10].

Using the equation (1) for locked rotor machines, the orientation problem can be solved in two steps:

First, with the rotor not fixed, a fixed current pointer is applied for rough alignment. The machine aligns itself in such a way that the d-axis is approximately in the direction of the chosen current pointer.

Next, the motor is locked in this position. Subsequently, a rotating voltage pointer is applied, and the voltage is steadily increased until an elliptical current curve can be seen in a rotor fixed coordinate system. The same voltage pointer is then applied again with a negative rotational direction. Fig. 1 shows the simulation result for an ideally aligned machine.

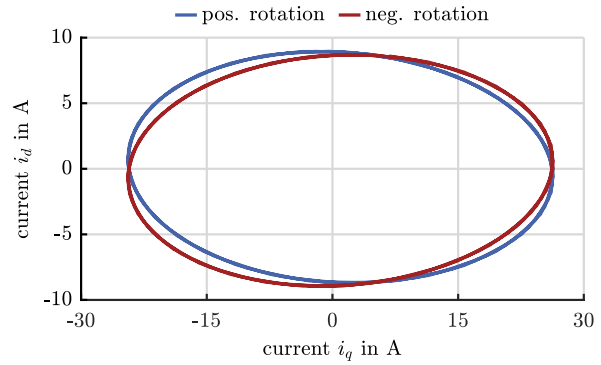

Fig. 1. Simulation results of ideal alignment.

Here it can be seen that due to the symmetry of the machine properties to the q-axis, both ellipses intersect on the d-axis if ideally aligned. However, this requires that the machine has anisotropy or can be saturated with positive d-current and thus anisotropy can be forced.

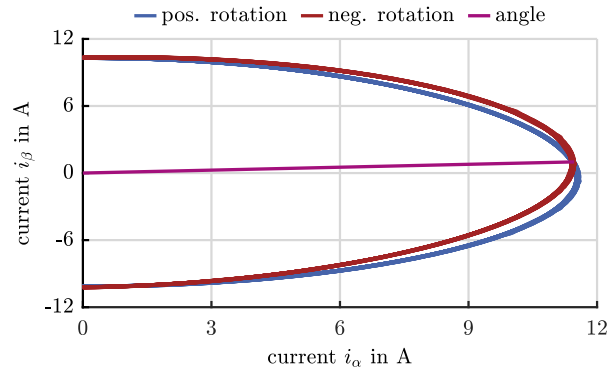

Fig. 2. Alignment of the used testbench and DUT.

Fig. 2 shows the initial alignment for the chosen DUT (machine Data in table II). The alignment was performed with a switching frequency of 8kHz, a voltage amplitude of 4V and a frequency of 300Hz.

Due to the relatively high electrical frequency, the control voltage can be increased and thus the influence of the voltage errors caused by the power converter can be reduced. In addition, the inductive voltage drop leads to an additional rotation of the current ellipsis, which makes evaluation of the intersection point more convenient.

B. Parameter Identification

The machine is first locked in a defined rotor position. Then, a 2-level converter is used to feed a three-phase current with defined amplitude and frequency. The currents and voltages are measured at high frequency and precision by the respective sensors and AD converters. Afterwards, the voltages and currents are transformed into the rotorflux-oriented coordinate system (Park-transformation) and subsequently Fourier-transformed. Fig. 3 shows the d-current at 2 kHz PWM and 100 Hz fundamental frequency.

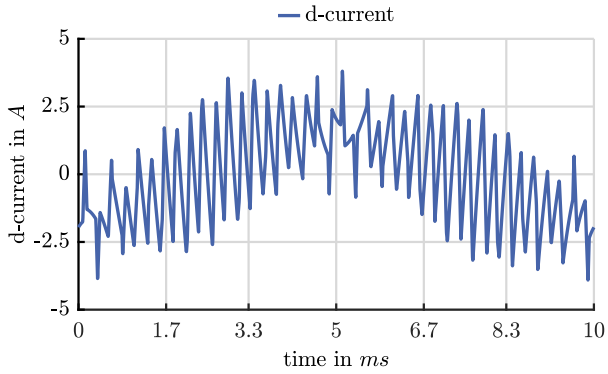

Fig. 3. DUT d-current at 2 kHz switching frequency.

Fig. 4 shows the spectrum of the d-current. Due to the modulation process, sideband harmonics by multiples of the switching frequency occur [11, 12]. Since the frequency of the fundamental wave (f_{el}) can be assumed to be low compared to the PWM frequency (f_{PWM}), the dominant sideband harmonics in the spectrum are relatively close to each other.

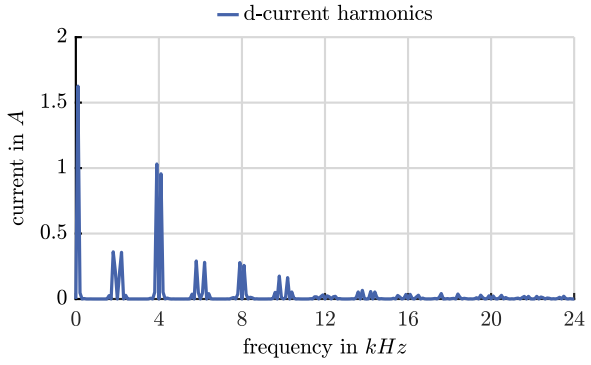

Fig. 4. Spectrum of the d-current shown in fig. 3.

It is therefore expected that the machine behaves approximately equal for each of these two sideband harmonics if the frequency difference is small compared to the actual frequency of each harmonic.

$$\begin{bmatrix} \Re\{u_{\mathrm{d,l}}\} \\ \Im\{u_{\mathrm{d,l}}\} \\ \Re\{u_{\mathrm{q,l}}\} \\ \Im\{u_{\mathrm{q,l}}\} \\ \Re\{u_{\mathrm{d,h}}\} \\ \Im\{u_{\mathrm{d,h}}\} \\ \Re\{u_{\mathrm{q,h}}\} \\ \lfloor \Im\{u_{\mathrm{q,h}}\} \rfloor \end{bmatrix} = \begin{bmatrix} \Re\{i_{\mathrm{d,l}}\} & \Re\{i_{\mathrm{q,l}}\} & 0 & 0 & -\Im\{i_{\mathrm{d,l}}\} & -\Im\{i_{\mathrm{q,l}}\} & 0 \\ \Im\{i_{\mathrm{d,l}}\} & \Im\{i_{\mathrm{q,l}}\} & 0 & 0 & \Re\{i_{\mathrm{d,l}}\} & \Re\{i_{\mathrm{q,l}}\} & 0 \\ 0 & 0 & \Re\{i_{\mathrm{d,l}}\} & \Re\{i_{\mathrm{q,l}}\} & 0 & -\Im\{i_{\mathrm{d,l}}\} & -\Im\{i_{\mathrm{q,l}}\} \\ 0 & 0 & \Im\{i_{\mathrm{d,l}}\} & \Im\{i_{\mathrm{q,l}}\} & 0 & \Re\{i_{\mathrm{d,l}}\} & \Re\{i_{\mathrm{q,l}}\} \\ \Re\{i_{\mathrm{d,h}}\} & \Re\{i_{\mathrm{q,h}}\} & 0 & 0 & -\Im\{i_{\mathrm{d,h}}\} & -\Im\{i_{\mathrm{q,h}}\} & 0 \\ \Im\{i_{\mathrm{d,h}}\} & \Im\{i_{\mathrm{q,h}}\} & 0 & 0 & \Re\{i_{\mathrm{d,h}}\} & \Re\{i_{\mathrm{q,h}}\} & 0 \\ 0 & 0 & \Re\{i_{\mathrm{d,h}}\} & \Re\{i_{\mathrm{q,h}}\} & 0 & -\Im\{i_{\mathrm{d,h}}\} & -\Im\{i_{\mathrm{q,h}}\} \\ \lfloor 0 & 0 & \Im\{i_{\mathrm{d,h}}\} & \Im\{i_{\mathrm{q,h}}\} & 0 & \Re\{i_{\mathrm{d,h}}\} & \Re\{i_{\mathrm{q,h}}\} \rfloor \end{bmatrix} \cdot \begin{bmatrix} R_{\mathrm{dd}} \\ R_{\mathrm{dq}} \\ R_{\mathrm{qd}} \\ R_{\mathrm{qq}} \\ L_{\mathrm{dd}} \\ L_{\mathrm{dq}} \\ \lfloor L_{\mathrm{qq}} \rfloor \end{bmatrix} \quad (3)$$

This allows combination of these two harmonics to be used during evaluation. To keep the deviations as small as possible, the switching harmonics with the smallest difference are therefore selected for the evaluation.

The harmonics in stator-fixed currents and voltages can be divided into two groups at the 2-level inverter [11]. For the odd-numbered multiples of the switching frequency, the sideband harmonics with the smallest frequency difference are each at $(2n-1)\cdot f_{\mathrm{PWM}} \pm 2f_{el}$ [11]. When evaluating this group, the two harmonics in the spectrum would therefore differ by at least $4\cdot f_{el}$.

In the evaluation of the even-numbered multiples of the switching frequency, the difference of the closest harmonics is only $2\cdot f_{el}$ [11]. Therefore, the following frequencies are selected for evaluation:

$$f_{\mathrm{harm}} = n\cdot 2\cdot f_{\mathrm{PWM}} \pm f_{el} \quad \text{for } n \in \mathbb{Z}_+ \qquad (2)$$

Through the complex representation of the Fourier transformation, these harmonics can be decomposed into a real and an imaginary part. This leads to the following system of equations (3). The index "h" represents the upper frequency sideband harmonic, the index "l" the lower frequency sideband harmonic. The system of equations is computed for each pair of sideband harmonics located in the vicinity and solved with Matlab® using *mldivide*. Fig. 5 shows the machine parameters for one rotor angle at 2 kHz PWM frequency and 100 Hz fundamental frequency. The graph shows the calculated parameters for one rotor angle. Each marker of the curve represents a solved system of equations.

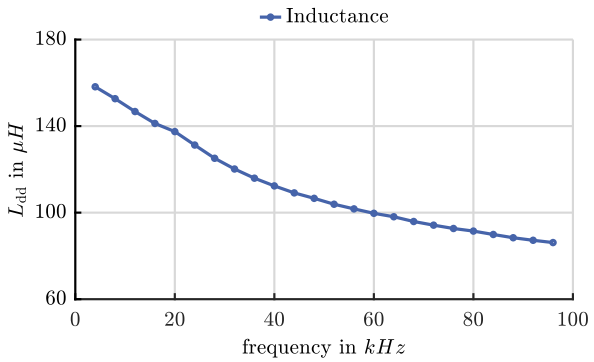

Fig. 5. Inductance L_{dd} of the d-axis for one measurement at 0°.

In order to determine the parameters as a function of the rotor position, the rotor is fixed in a new position and the measurement is repeated until one electrical or mechanical period is identified. Due to the over determinedness of the equation system, noise can be reduced resulting in a stable solution.

C. Current Controller

To ensure a constant current amplitude even at high frequencies of the fundamental wave during the measurement of the DUT, the controller was implemented in a rotating reference frame similar to the field-oriented control of the PMSM or induction motor [13]. As the reference frame is not rotor orientated, the axes are designated x and y instead of d and q on the PMSM. To set a constant amplitude, the y-current is set to 0 A and the x-current corresponds to the desired current amplitude.

Since the DUT has angle-dependent machine characteristics and the various commutation processes cause voltage errors in the converter, it is not possible to achieve a smooth sinusoidal current using classical PI control in a rotating coordinate system. To enable a measurement at a constant operating point, a repetitive PI control was used. The structure of the controller corresponds in principle to the results from [14], but instead of using a model-based controller, the proportional and integral gain components were selected on the basis of the adjustment rules of the method of gain optimum [15].

In simplified terms, the control system consists of different PI controllers, which are all designed according to the basic DUT parameters and the method of gain optimum. The used controller is selected depending on the present angular segment of the transformation angle. The transformation angle is determined by the rotation angle of the rotating coordinate system of the controller.

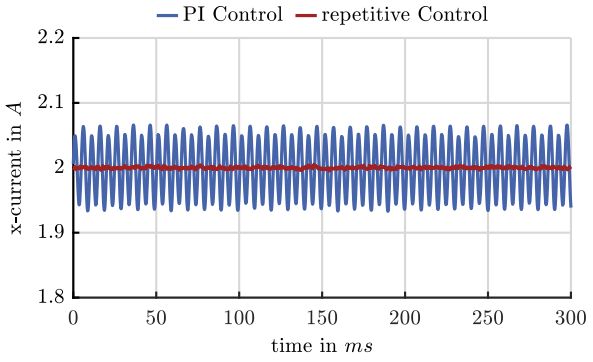

Fig. 6. Impact of the repetitive PI controller on the harmonics of the y-current at 8 kHz.

Since the integral components of the different controllers now gradually reduce the control deviation for each angular segment, this structure significantly reduces the harmonics in the current and enables improved parameter identification through a constant operating point. Fig. 6 shows the impact of the introduced control structure on the currents in rotating reference frame.

D. *Sampling frequency and bandwidth*

When analysing data in the frequency domain, distortions occur due to the spectral leakage. This effect occurs when a signal can only be analysed over a limited observation period and is therefore windowed [16]. This influence can be prevented by suitable windowing of the signal. In the given scenario, only multiple of whole electrical periods were examined. The frequency of the fundamental wave was selected to ensure that it always corresponds to an integer divisor of the switching frequency. In this way, leakage can be prevented effectively.

Since the measurement data can be additionally distorted by low-pass filters, no high order anti-aliasing filters can be used. To estimate the error that could be caused by the violation of the sampling theorem, a simple general example for this evaluation principle is given below.

Therefore, a model with an ideal inductance with 0.5 H is excited with a square-wave signal of 1 V amplitude and a frequency of 1Hz. This signal is then sampled at 50 Hz sample rate (fig.7), transformed into the frequency domain and analysed. Since the inductance is not frequency-dependent, the evaluation should result in a constant inductance in the frequency range of 0.5 H.

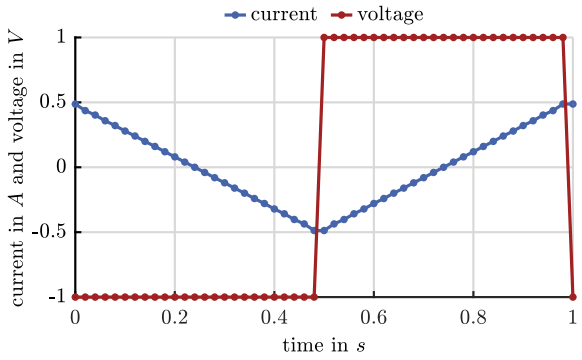

Fig. 7. Simulation of current and voltage for a constant inductance with 0.5 H.

Due to the neglection of the sampling theorem, there is a deviation in the frequency domain, which corresponds to about 35% of the inductance value at the Nyquist frequency. The data can be seen in fig. 8. These effects should be taken into account when choosing the sample rate, PWM frequency and maximum evaluation frequency, as the effects on the result are comparable to the HF characteristics of the machine and can therefore falsify the results.

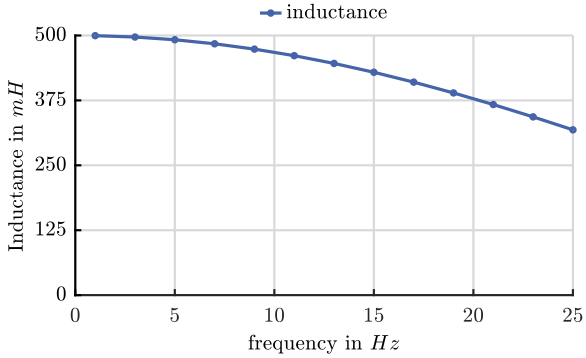

Fig. 8. Frequency behaviour of the inductance under neglect of the sampling theorem.

Based on the shown approximation, the measurement error in this paper is expected to be at around 0.07 % based on 5 MHz sample rate and 100 kHz maximum evaluation frequency. Since the DUT has a low-pass characteristic and low order anti-aliasing filters are installed within the measurement system, a significantly lower deviation is to be expected at the test setup.

IV. Testbench Setup

The measurements were carried out with the inverter presented in [17] with its hardware properties listed in Table I

TABLE I. Technical Specifications of the Inverter [17]

Symbol	Meaning	value
$P_{\max}$	maximum power	1.4 kW
$V_{\mathrm{DC,max}}$	Maximum DC link voltage	60 V
f_{PWM}	Maximum PWM frequency	100 kHz
i_{max}	Maximum phase current	25 A

A. *Sensors and signal processing*

For good noise immunity, the current measurement on the test bench is carried out by *LEM LAH25NP* current sensors with a current output, as this offers improved noise immunity against coupling compared to sensor with voltage output. For these sensors, the maximum amplitude error is less than 3% and the maximum phase error is approx. 1° for a frequency range up to 100kHz [18]. The output current of the sensor is then converted into a ±10V voltage signal by a load resistor and a differential amplifier with lowpass using the *Analog Devices - ADA 4898*. The output voltage of the power converter is directly converted into a voltage range of ±10V by a differential amplifier circuit using the *Texas Instruments THS4131* with a cut-off frequency of 2.5MHz. The output voltages of the current and voltage measurements are subsequently converted by the AD card of the ETI SoC system shown in [19]. It is equipped with the *Analog Devices LTC2325* 16bit, 5MSPS AD converter and thus offers sufficient measurement accuracy and bandwidth.

B. *Locked Rotor test bench*

Fig. 9 shows the test setup. This consists of the power converter, the ETI-SoC system and the locked rotor test bench.

Fig. 9. Testbench with ETI – SoC System (right) [19], inverter [17] and the locked rotor testbench (left).

The locked rotor test bench consists of a fixed part, which is connected to the test bench bed, and a rotating part, which is locked by 2 screws. This can be seen in the picture on the left. Both parts have 10 holes each, which are shifted by 10° in the fixed part and 11° in the rotating part. By combining the holes, defined angles can be selected in 1° steps.

TABLE II. MACHINE DATA OF NANOTEC DB59M024035R [20]

Symbol	Meaning	value
P_N	Nominal power	135 W
V_N	Nominal voltage	24 V
I_N	Nominal current	8 A
p	Pole pairs	3
R_s	Stator resistance	120 mΩ
L_d	d inductance	0.15 mH
L_q	q inductance	0.15 mH
Ψ_{PM}	PM flux linkage	11.7 mVs

Table II gives an overview of the machine characteristics of the DUT based on the datasheet. Since the rotor is equipped with surface magnets, it is assumed that the inductance in the d- and q-axis are identical.

V. MEASUREMENT RESULTS

In this chapter the results of this procedure without any additional filtering or smoothing are shown. Due to the large frequency range of the harmonics, an identification with a bandwidth of more than 100 kHz can be carried out in one step. All measurements covered current amplitudes from 2 A to 6 A. In the following subsections, the analysis of one amplitude is presented in detail.

To demonstrate the performance of the identification, individual measurement results at different switching frequencies are presented below. In this context, 8 kHz is a typical switching frequency for automotive and small industrial applications, while 2 kHz is more common for large industrial drives.

A. Measurements at 2kHz PWM frequency

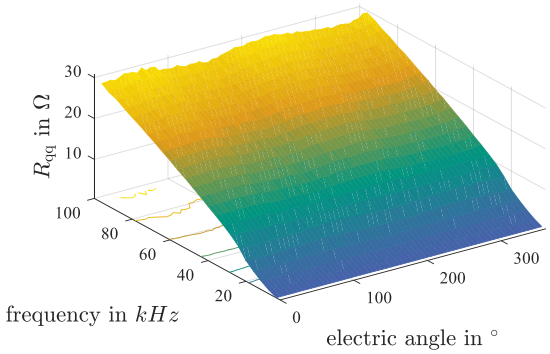

Fig. 9. Resistance R_{qq} at 2 kHz PWM Frequency and 100 Hz fundamental frequency.

First, measurements were carried out at a switching frequency of 2 kHz with an angular resolution of 6° electrically and an electrical frequency of 100 Hz. The graphs in this section present the results for a fundamental amplitude of 2 A. The repetitive PI control was operated with 12 different integrators. Each operating point, defined by the current amplitude and angle was evaluated with a duration of 4 electrical periods consisting of 200.000 sample points.

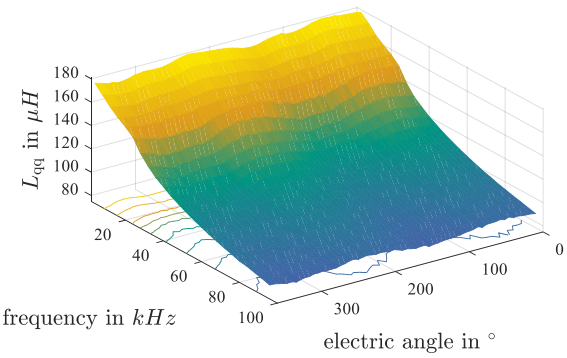

Fig. 10. Inductance L_{qq} at 2 kHz PWM Frequency and 100 Hz fundamental frequency.

In the range of 25 kHz a resonance in the motor can be observed for 2 kHz PWM frequency, which is reflected differently in the resistances R_{qd} and R_{dq} and also by a phase shift of the inductance L_{qd} and can be seen in fig. 11.

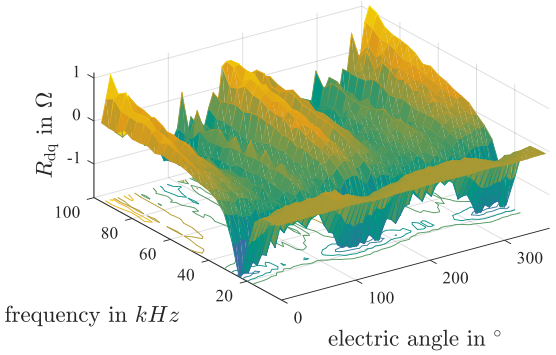

Fig. 11. Resistance R_{dq} at 2 kHz PWM Frequency and 100 Hz fundamental frequency.

B. Measurements at 8 kHz PWM frequency

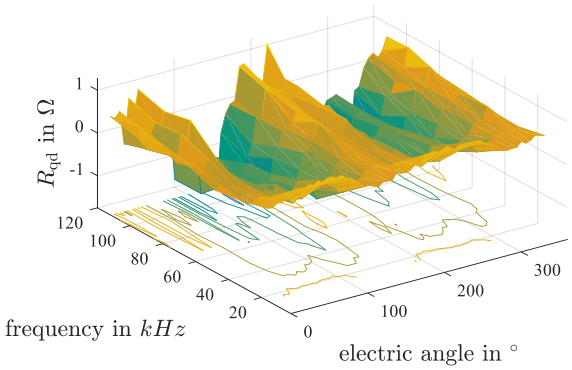

Fig. 12. Resistance R_{qd} at 8 kHz PWM Frequency and 100 Hz fundamental frequency.

Measurements at 8 kHz switching frequency were carried out with an angular resolution of 6° electrically and an electrical frequency of 100 Hz. The graphs in this section present the results for a fundamental amplitude of 4 A. The repetitive PI control was operated with 12 different integrators.

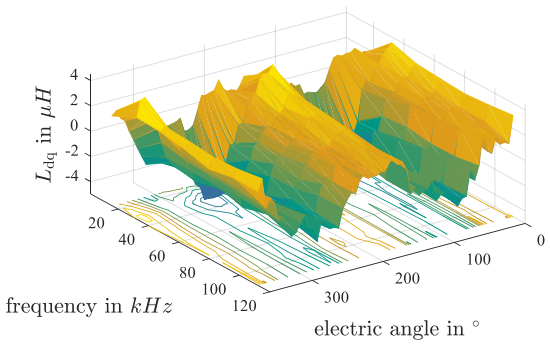

Fig. 13. Inductance L_{dq} at 8 kHz PWM Frequency and 100 Hz fundamental frequency.

Due to the higher switching frequency, an evaluation of the measurement is even possible at frequencies above 100 kHz. However, deviations in the measurement results may occur due to the reduced sensor accuracy of the current measurement.

VI. Conclusionand Future Work

In this paper, a method for the angle-dependent measurement of HF machine parameters based on switching harmonics of the 2-level inverter was presented. First measurements have been conducted on the testbench presented in [17], demonstrating the technical feasibility of the presented procedure. The measurements demonstrate the significant increase of the measurement bandwidth as well as of the maximum evaluation frequency by a factor of 50 compared to known methods [1].

The analysis reveals that the angular dependence of all parameters is usually more prominent at high frequencies. This may allow further improvement of sensorless control algorithms by increasing the detection frequency. Furthermore, parameter identification methods based on 2-level inverter induced current slopes [21] could also be extended by taking frequency dependences of parameter into account.

VII. References

[1] M. O. Zapico, D. D. Reigosa, D. F. Laborda, M. M. Gomez, J. M. G. Munoz, and F. B. d. Blanco, "Use HF Signal Injection for Simultaneous Rotor Angle, Torque and Temperature Estimation in PMSMs," in *ECCE 2021: 2021 IEEE Energy Conversion Congress & Exposition : virtual conference, Oct. 10-14 : proceedings*, Vancouver, BC, Canada, 2021, pp. 5084–5091.

[2] M. Seilmeier, S. Ebersberger, and B. Piepenbreier, "Identification of high frequency resistances and inductances for sensorless control of PMSM," in *2013 IEEE International Symposium on Sensorless Control for Electrical Drives and Predictive Control of Electrical Drives and Power Electronics (SLED/PRECEDE 2013): United symposium] ; Munich, Germany, 17 - 19 October 2013*, München, Germany, 2013, pp. 1–8.

[3] L. Alberti, N. Bianchi, M. Morandin, and J. Gyselinck, "Finite-element analysis of electrical machines for sensorless drives with signal injection," in *2012 IEEE Energy Conversion Congress and Exposition (ECCE 2012): Raleigh, North Carolina, USA, 15 - 20 September 2012*, Raleigh, NC, USA, 2012, pp. 861–868.

[4] D. Reigosa, D. Fernandez, M. Martinez, J. M. Guerrero, A. B. Diez, and F. Briz, "Magnet Temperature Estimation in Permanent Magnet Synchronous Machines Using the High Frequency Inductance," *IEEE Trans. on Ind. Applicat.*, vol. 55, no. 3, pp. 2750–2757, 2019, doi: 10.1109/TIA.2019.2895557.

[5] D. D. Reigosa, D. Fernandez, H. Yoshida, T. Kato, and F. Briz, "Permanent-Magnet Temperature Estimation in PMSMs Using Pulsating High-Frequency Current Injection," *IEEE Trans. on Ind. Applicat.*, vol. 51, no. 4, pp. 3159–3168, 2015, doi: 10.1109/TIA.2015.2404922.

[6] P. Garcia, F. Briz, D. Reigosa, C. Blanco, and J. M. Guerrero, "On the use of high frequency inductance vs. high frequency resistance for sensorless control of AC machines," in *Symposium on Sensorless Control for Electrical Drives (SLED 2011): 1 - 2 Sept. 2011, Birmingham, UK*, Birmingham, United Kingdom, 2011, pp. 90–95.

[7] M. W. Degner and R. D. Lorenz, "Using multiple saliencies for the estimation of flux, position, and velocity in AC machines," *IEEE Trans. on Ind. Applicat.*, vol. 34, no. 5, pp. 1097–1104, 1998, doi: 10.1109/28.720450.

[8] M. Martinez, D. Reigosa, D. Fernandez, J. M. Guerrero, and F. Briz, "PMSMs Torque Estimation Using Pulsating HF Current Injection," in *SLED 2018: 2018 IEEE 9th International Symposium on Sensorless Control for Electrical Drives (SLED) : September 13-14, 2018, Helsinki, Finland*, Helsinki, 2018, pp. 96–101.

[9] P. L. Xu and Z. Q. Zhu, "Comparison of carrier signal injection methods for sensorless control of PMSM drives," in *2015 IEEE Energy Conversion Congress and Exposition (ECCE 2015): Montreal, Quebec, Canada, 20 - 24 September 2015*, Montreal, QC, Canada, 2015, pp. 5616–5623.

[10] P. L. Jansen and R. D. Lorenz, "Transducerless position and velocity estimation in induction and salient AC machines," *IEEE Trans. on Ind. Applicat.*, vol. 31, no. 2, pp. 240–247, 1995, doi: 10.1109/28.370269.

[11] M. Brenna, R. Chiumeo, and C. Gandolfi, "Harmonic analysis: Comparison between different modulation strategies for three phase inverter connecting Distributed Generation," in *2011 International Conference on Clean Electrical Power (ICCEP 2011): Ischia, Italy, 14 - 16 June 2011*, Ischia, Italy, 2011, pp. 231–236.

[12] W. Liang, J. Wang, and W. Fang, "Analytical Modeling of Sideband Current Harmonic Components in Induction Machine Drive With Voltage Source Inverter by an SVM Technique," *IEEE Trans. Power Electron.*, vol. 28, no. 11, pp. 5372–5379, 2013, doi: 10.1109/TPEL.2013.2238643.

[13] *Das verfahren der feldorientierung zur regelung der asynchronmaschine*, 1972.

[14] J. Richter, T. Lannert, T. Gemassmer, and M. Doppelbauer, "Mitigation of Current Harmonics in Inverter-Fed Permanent Magnet Synchronous Machines with Nonlinear Magnetics," in *Proceedings of PCIM Europe 2015; International Exhibition and Conference for Power Electronics, Intelligent Motion, Renewable Energy and Energy Management*, 2015, pp. 1–8.

[15] A. L. Whiteley, "Theory of servo systems, with particular reference to stabilization," *Journal of the Institution of Electrical Engineers - Part II: Power Engineering*, vol. 93, no. 34, pp. 353–367, 1946, doi: 10.1049/ji-2.1946.0083.

[16] F. J. Harris, "On the use of windows for harmonic analysis with the discrete Fourier transform," *Proc. IEEE*, vol. 66, no. 1, pp. 51–83, 1978, doi: 10.1109/PROC.1978.10837.

[17] Stoß Johannes, Wurster Christoph, Menger Nikolas, Brodatzki Matthias, Liske Andreas, and Hiller Marc, "Design guideline for PCB integrated, high bandwidth, current slope sensing based on a planar Rogowski coil," in *2021 23rd European Conference on Power Electronics and Applications (EPE'21 ECCE Europe)*, 2021, pp. 1–10.

[18] LEM, *Elektronische Komponenten - Kompensations-Stromwandler mit kleiner Montageflaeche bis 100-A-Nennstrom.* [Online]. Available: https://www.lem.com/images/stories/files/Products/P1_5_1_industry/CH99102D.pdf (accessed: Sep. 28 2022).

[19] B. Schmitz-Rode *et al.,* "A modular signal processing platform for grid and motor control, HIL and PHIL applications," in *2022 International Power Electronics Conference (IPEC-Himeji 2022-ECCE Asia)*, Himeji, Japan, May. 2022 - May. 2022, pp. 1817–1824.

[20] Nanotec, "Datasheet DB59M024035R-B3," [Online]. Available: https://de.nanotec.com/fileadmin/files/Datenblaetter/BLDC/DB59-rund/DB59M-R/DB59M024035R-B3.pdf

[21] S. Decker, J. Stoss, A. Liske, M. Brodatzki, J. Kolb, and M. Braun, "Online Parameter Identification of Permanent Magnet Synchronous Machines with Nonlinear Magnetics based on the Inverter Induced Current Slopes and the dq-System Equations," in *2019 21st European Conference on Power Electronics and Applications (EPE '19 ECCE Europe)*, Genova, Italy, 2019, P.1-P.10.